Biomaterials Science

PAPER

View Article Online
View Journal | View Issue

Cite this: *Biomater. Sci.*, 2017, **5**, 1828

Iodine-131-labeled, transferrin-capped polypyrrole nanoparticles for tumor-targeted synergistic photothermal-radioisotope therapy†

Xuejiao Song,‡[a] Chao Liang,‡[a] Liangzhu Feng,[a] Kai Yang*[b] and Zhuang Liu *[a]

Combining different therapeutic functions within single tumor-targeted nanoscale delivery systems is promising to overcome the limitations of conventional cancer therapies. Herein, transferrin that recognizes transferrin receptors up-regulated on tumor cells is pre-labeled with iodine-131 (^{131}I) and then utilized as the stabilizer in the fabrication of polypyrrole (PPy) nanoparticles. The obtained transferrin-capped PPy@Tf-^{131}I nanoparticles could be used for tumor-targeted radioisotope therapy (RIT) and photothermal therapy (PTT), by employing beta-emission from ^{131}I and the intrinsic high near-infrared (NIR) absorbance of PPy, respectively. Owing to the transferrin-mediated tumor targeting, PPy@Tf-^{131}I nanoparticles exhibit obviously enhanced *in vitro* cancer cell binding and *in vivo* tumor uptake compared to its non-targeting counterpart. The combined RIT and PTT based on PPy@Tf-^{131}I nanoparticles is then conducted, achieving a remarkable synergistic therapeutic effect. This work thus demonstrates a rather simple one-step approach to fabricate tumor-targeting nanoparticles based on protein-capped conjugated polymers, promising for combination cancer therapy with great efficacy and high safety.

Received 4th May 2017,
Accepted 20th June 2017

DOI: 10.1039/c7bm00409e

rsc.li/biomaterials-science

Introduction

Cancer radiation therapy, also known as radiotherapy, in which ionization radiation is employed to destruct cancer, has been extensively used in clinics. Up to 50% cancer patients have received radiotherapy during their battle against cancers.[1–3] Apart from external beam radiotherapy (EBRT) with radiation beams (*e.g.* X-ray) applied onto tumors externally, internal radioisotope therapy (RIT) is another important type of cancer therapy carried out by the *in situ* implantation or administration of radioactive sources to irradiate tumors from inside the body.[4–6] Despite the extensive use of both EBRT and RIT in cancer treatment, there are tremendous clinical needs to further improve the treatment efficacy and specificity, as well as reduce the radiation damage to normal tissues during the treatment.

Recently, with the advances in nanotechnology, a large variety of radioisotope-labeled nanomaterials have been found to be able to efficiently accumulate in tumors *via* passive tumor targeting by the enhanced permeability and retention (EPR) effect, or active targeting by utilizing tumor-specific ligands, showing promising potential for internal RIT.[7–11] By combining RIT with other treatment methods such as chemotherapy within nanoscale platforms, the achieved therapeutic outcomes may be further optimized.[6,12–14] More recently, the idea of combining radiotherapy with photothermal therapy (PTT) using nano-theranostic agents has been also proposed for effective combination tumor treatment, considering that mild photothermal heating may be helpful in relieving tumor hypoxia *via* boosting intra-tumoral blood, so as to overcome the hypoxia-associated radio-resistance.[15,16] However, many of these previously reported nano-platforms for photothermal-radiotherapy have been based on inorganic non-biodegradable materials.[5,16–19] Moreover, in order to realize tumor-specific active targeting, tedious post-synthesis bioconjugation of targeting ligands onto nanoparticles is often required.[20–24] Therefore, the development of biocompatible tumor-targeted nano-agents that can be fabricated *via* easy procedures for such synergistic cancer combination therapy would be of great interest but demands further explorations.

Conjugated polymers are highly versatile materials and have been widely used in various areas including

[a]*Institute of Functional Nano & Soft Materials (FUNSOM), Jiangsu Key Laboratory for Carbon-Based Functional Materials & Devices, Soochow University, Suzhou 215123, China. E-mail: zliu@suda.edu.cn*
[b]*School of Radiation Medicine and Protection & School for Radiological and Interdisciplinary Sciences (RAD-X), Collaborative Innovation Center of Radiation Medicine of Jiangsu Higher Education Institutions Medical College of Soochow University, Suzhou, Jiangsu 21513, China. E-mail: kyang@suda.edu.cn*
†Electronic supplementary information (ESI) available. See DOI: 10.1039/c7bm00409e
‡These two authors contributed equally to this work.

nanomedicine.[25–27] Due to their strong and stable absorbance in the near-infrared (NIR) region, a number of conjugated polymers such as polyaniline and polypyrrole (PPy) have been developed as robust photothermal agents for tumor ablation therapy.[25,28–30] In a previous study by our group, albumin pre-conjugated with a photosensitizer was used as the stabilizer to synthesize multifunctional albumin-capped PPy nanoparticles,[31] which however had no active tumor-targeting ability. Inspired by that work, herein, we used radioisotope ^{131}I labeled transferrin (Tf), a tumor-targeting protein that specifically binds to its receptors over-expressed on various types of tumor cells,[32–34] as a stabilizing molecule to prepare Tf-capped PPy (PPy@Tf) nanoparticles *via* a one-step method (Fig. 1a). The obtained PPy@Tf-^{131}I nanoparticles showed *in vitro* specific uptake by tumor cells with an over-expressed Tf receptor (TfR), as well as efficient accumulation in TfR positive U87MG human glioblastoma tumors grown on mice after intravenous (i.v.) injection. Upon mild photothermal heating with a NIR laser on tumors, mice treated with PPy@Tf-^{131}I nanoparticles showed the most effective tumor growth inhibition effect *via* the synergistic photothermal-radioisotope therapy. Our results demonstrate a simple one-step approach for the fabrication of tumor-targeted multifunctional nano-theranostics for efficient tumor synergistic therapy.

Results and discussion

Transferrin (Tf), an iron-binding blood plasma glycoprotein, has been found to be an efficient tumor targeting moiety owing to the over-expression of its receptor, TfR, on the surface of various types of tumor cells.[35–38] In this work, Tf-^{131}I was prepared by labeling native Tf with ^{131}I *via* a standard chloramine-T oxidation method.[6] After the removal of excess ^{131}I, PPy@Tf or PPy@Tf-^{131}I nanoparticles were prepared *via* the Fe^{3+}-triggered self-polymerization of pyrrole, with Tf or Tf-^{131}I used as the capping agent to stabilize the obtained nanoparticles following our previously developed method to synthesize albumin-capped PPy nanoparticles (Fig. 1a).[31] Without the need for further surface modification, the obtained PPy@Tf and PPy@Tf-^{131}I nanoparticles exhibited great colloidal stability even in the presence of salts and serum proteins. On the other hand, the obtained PPy@Tf-^{131}I nanoparticles showed excellent labeling stability, with only 7% of radioactivity detachment after being incubated with phosphate buffer saline (PBS) and fetal bovine serum (FBS) for 5 days (ESI, Fig. S1†). For the safety reason, PPy@Tf without radioisotope labeling was used in the following experiments for detailed characterization.

Under a transmission electron microscope (TEM), the obtained PPy@Tf and PPy@BSA nanoparticles showed

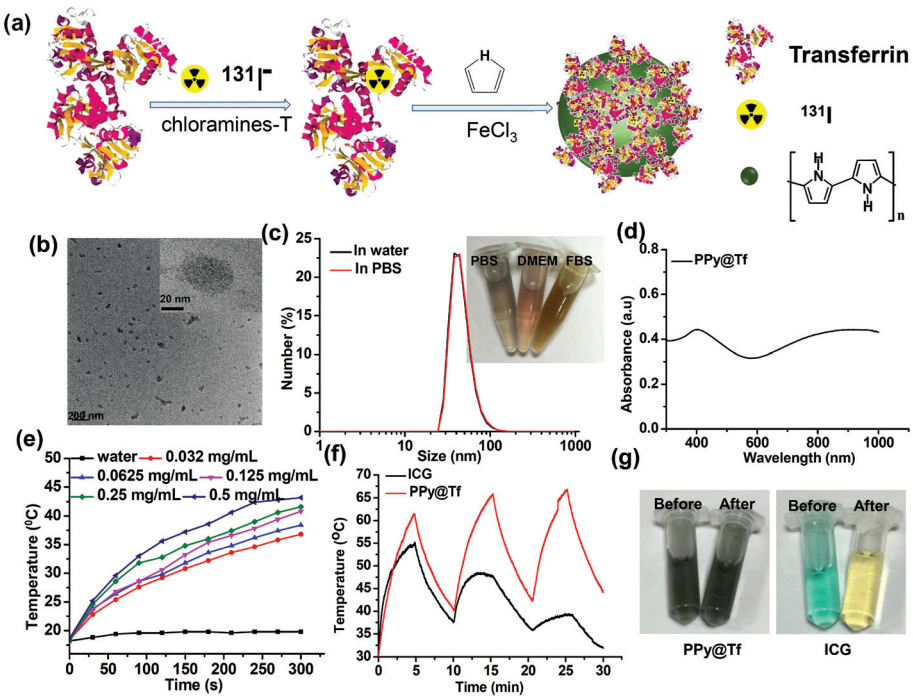

Fig. 1 Synthesis and characterization of PPy@Tf nanoparticles. (a) Schematic illustration of the fabrication of PPy@Tf-^{131}I. (b) A TEM image of the as-synthesized PPy@Tf nanoparticles. (c) Hydrodynamic diameters of PPy@Tf nanoparticles measured in water or PBS. The inset is a photo of PPy@Tf nanoparticles incubated in different physiological solutions. (d) UV-vis-NIR absorbance spectra of PPy@Tf nanoparticles in water. (e) Temperature elevation of water and PPy@Tf solutions at different concentrations over a period of 5 min under exposure to the NIR light (808 nm, 0.5 W cm^{-2}). (f) Temperature change curves of ICG (0.08 mg mL^{-1}) and PPy@Tf (0.125 mg mL^{-1}) solutions after multiple rounds of NIR laser irradiation. (e) Photos of ICG and PPy@Tf before and after laser irradiation. PPy@Tf showed much better photostability compared to ICG.

uniform size distribution (Fig. 1b and ESI, Fig. S2†). By utilizing dynamic light scattering (DLS), it was found that the mean size of the as-prepared PPy@Tf nanoparticles was about 50 nm (Fig. 1c), consistent with the TEM observation. In their UV-vis-NIR spectrum, PPy@Tf nanoparticles showed a broad and strong absorption band ranging from the visible to the NIR region (Fig. 1d). Owing to their high NIR absorbance, PPy@Tf nanoparticles showed a great photothermal conversion ability under the irradiation of an 808 nm NIR laser (Fig. 1e). Moreover, unlike small organic dye molecules such as indocyanine green (ICG), the PPy@Tf nanoparticles showed a great photothermal ability without losing their NIR absorbance even after multiple rounds of NIR laser irradiation (Fig. 1f & g).

Then, the TfR-specific targeting ability of the as-prepared PPy@Tf nanoparticles was evaluated by incubating fluorescein labeled PPy@Tf (PPy@Tf-FITC) with U87MG cancer cells over-expressing TfR and normal 293T cells. PPy nanoparticles stabilized with bovine serum albumin (BSA) and labeled with fluorescein were also prepared as the control. Under a confocal laser scanning microscope (CLSM), we observed that U87MG cells incubated with PPy@Tf-FITC nanoparticles showed strong fluorescence signals, while rather weak fluorescence signals were observed for cells with TfR pre-blocked by native Tf before being incubated with PPy@Tf-FITC, as well as cells incubated with PPy@BSA-FITC nanoparticles (Fig. 2a). Moreover, the TfR-specific targeting ability of PPy@Tf nanoparticles was also investigated by flow cytometric analysis. U87MG cells and TfR negative 293T cells were incubated with PPy@Tf-FITC, PPy@BSA-FITC, and PPy@Tf-FITC with Tf pre-blocked (PPy = 0.1 mg mL^{-1}) (Fig. 2b & ESI Fig. S3†). Similar results further demonstrated that our PPy@Tf nanoparticles were able to target cancer cells with TfR over-expression *via* the specific Tf/TfR recognition.

Next, the cytotoxicity of such PPy@Tf nanoparticles to U87MG cells and 293T cells was studied using the standard thiazolyl tetrazolium (MTT) assay. It was found that PPy@Tf nanoparticles showed negligible cytotoxicity to the U87MG cells and 293T cells even at high concentrations of up to 200 mg L^{-1} for 24 h (ESI Fig. S4†), indicating the excellent biocompatibility of the protein-capped PPy nanoparticles. The targeted cell killing ability of radioisotope labeled nanoparticles was then evaluated by incubating U87MG cells with free ^{131}I, PPy@Tf-^{131}I, or PPy@BSA-^{131}I at different radioactivity doses for 1 h. After additional 24 h incubation within fresh cell culture medium, it was found that only PPy@Tf-^{131}I nanoparticles showed dose-dependent cytotoxicity to the treated U87MG cells while both free ^{131}I and PPy@BSA-^{131}I did not show significant cytotoxicity to the cells under the same experimental conditions (Fig. 2c), demonstrating the capability of our PPy@Tf-^{131}I nanoparticles for TfR-targeted RIT. Furthermore, owing to the excellent photothermal conversion ability of such PPy@Tf nanoparticles, we found that U87MG

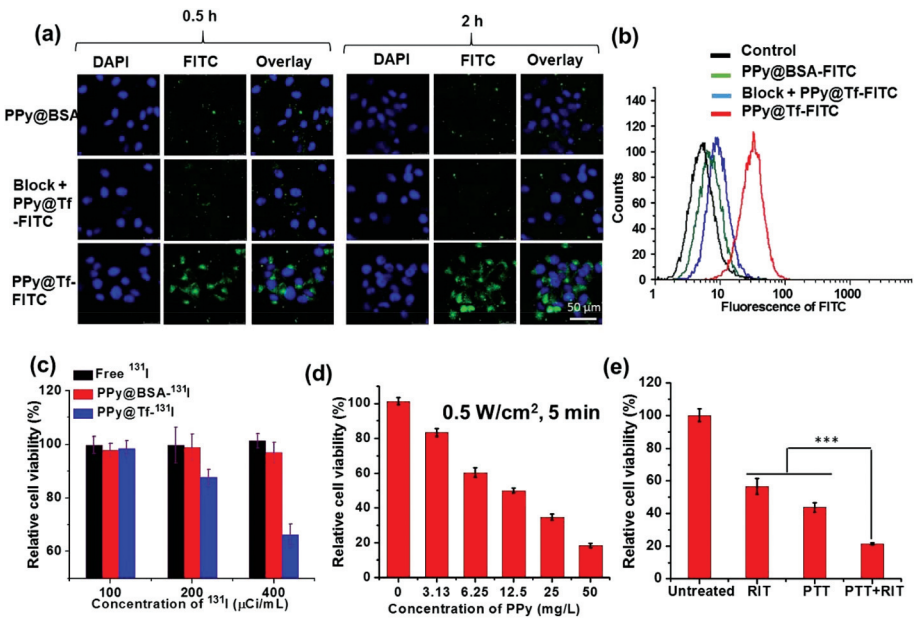

Fig. 2 *In vitro* cancer cell targeting and combination therapy. (a) Confocal fluorescence images of U87MG cells after incubation with PPy@BSA-FITC or PPy@Tf-FITC. As another control, U87MG cells pre-incubated with excess Tf to block the TfR for 1 h were added with PPy@Tf-FITC for further incubation (block + PPy@Tf-FITC). (b) Flow cytometry data for U87MG cells incubated with PPy@BSA-FITC or PPy@Tf-FITC for 1 h. TfR blocked U87MG cells incubated with PPy@Tf-FITC (block + PPy@Tf-FITC) were introduced as another control. (c) Relative viabilities of U87MG cells treated with free ^{131}I, PPy@BSA-^{131}I, or PPy@Tf-^{131}I at different concentrations of ^{131}I. (d) Relative viabilities of U87MG cells incubated with PPy@Tf at different concentrations of PPy under the 808 nm laser irradiation (0.5 W cm^{-2}, 5 min). (e) *In vitro* combined PTT and RIT. For RIT, cancer cells were incubated with PPy@Tf-^{131}I (dose of ^{131}I = 200 μCi mL^{-1}) for 24 h. For PTT, cancer cells were incubated with the same concentration of PPy@Tf (dose of PPy = 12.5 mg L^{-1}) and treated by the 808 nm laser irradiation (0.5 W cm^{-2}, 5 min). Relative cell viabilities in comparison with those of untreated cells are presented in the data. *P* values: $^{**}P < 0.01$, $^{***}P < 0.001$, ANOVA.

cells incubated with PPy@Tf nanoparticles showed a concentration dependent photothermal cell killing effect upon exposure to an 808 nm laser for 5 min (Fig. 2d). Afterwards, the combinational therapeutic effect of PPy@Tf-^{131}I nanoparticles was evaluated. Compared to the cells treated with PPy@Tf-^{131}I nanoparticles without light exposure, or PPy@Tf nanoparticles plus photothermal treatment (808 nm, 0.5 W cm^{-2}, 5 min), the cells incubated with PPy@Tf-^{131}I nanoparticles plus NIR laser irradiation under the same conditions showed drastically reduced cell viability (Fig. 2e). Therefore, our results indicate that such PPy@Tf-^{131}I nanoparticles could be used for the combined photothermal-radioisotope therapy.

Considering that ^{131}I is able to emit both beta particles and gamma rays, we used gamma imaging to track PPy@Tf-^{131}I nanoparticles within the U87MG tumor-bearing nude mice after intravenous (i.v.) injection. PPy@Tf-^{131}I nanoparticles showed obvious tumor accumulation at 24 h post-injection (p.i.), to a level much higher than that of PPy@BSA-^{131}I nanoparticles without the TfR targeting ability (Fig. 3a & ESI Fig. S5†). In contrast, most of the free ^{131}I after i.v. injection would be rapidly excreted from mice *via* the renal pathway without showing any appreciable accumulation in tumors. Moreover, the detailed *in vivo* pharmacokinetic behaviors of the as-prepared PPy@Tf-^{131}I and PPy@BSA-^{131}I nanoparticles were further studied using a gamma counter. The blood circulation half-lives of PPy@BSA-^{131}I and PPy@Tf-^{131}I were calculated to be 4.99 h and 5.54 h and their areas-under-curve (AUCs) were calculated to be 636 and 648 mCi h L^{-1}, respectively. Both PPy@Tf-^{131}I and PPy@BSA-^{131}I nanoparticles after i.v. injection showed no significant difference in terms of their blood circulation profiles (Fig. 3b). Additionally, the detailed biodistribution of such PPy@Tf-^{131}I and PPy@BSA-^{131}I nanoparticles in U87MG tumor bearing mice was determined at 24 h p.i. (Fig. 3c). The tumor accumulation of PPy@Tf-^{131}I nanoparticles was measured to be ~3 fold compared to that of PPy@BSA-^{131}I nanoparticles. Notably, the radioactivity levels in other normal organs of PPy@BSA-^{131}I injected mice appeared to be quite low (below ~5% ID g^{-1} even for the liver). These results collectively demonstrate that our PPy@Tf-^{131}I nanoparticles have a remarkable active tumor targeting ability, promising for further tumor-targeted treatment.

Motivated by the excellent *in vitro* cell killing efficacy of the combined PTT–RIT, as well as the active tumor targeting ability of such PPy@Tf-^{131}I, the *in vivo* combined RIT–PTT treatment with PPy@Tf-^{131}I nanoparticles was then evaluated. U87MG tumor bearing mice with tumor sizes of ~75 mm^3 were randomly divided into four groups as follows: (I) control group with saline injection only; (II) PTT group with PPy@Tf nanoparticle injection plus 808 nm laser irradiation; (III) RIT group with PPy@Tf-^{131}I nanoparticle injection only, and (IV) combination group with PPy@Tf-^{131}I nanoparticle injection plus 808 nm laser irradiation. The dose of ^{131}I was 300 μCi per mouse for all RIT groups. NIR laser irradiation was carried out 24 h post i.v. injection of nanoparticles, by exposing the mice to an 808 nm laser for 20 min (power density = 0.5 W cm^{-2}) with their tumor surface temperature controlled at ~45 °C

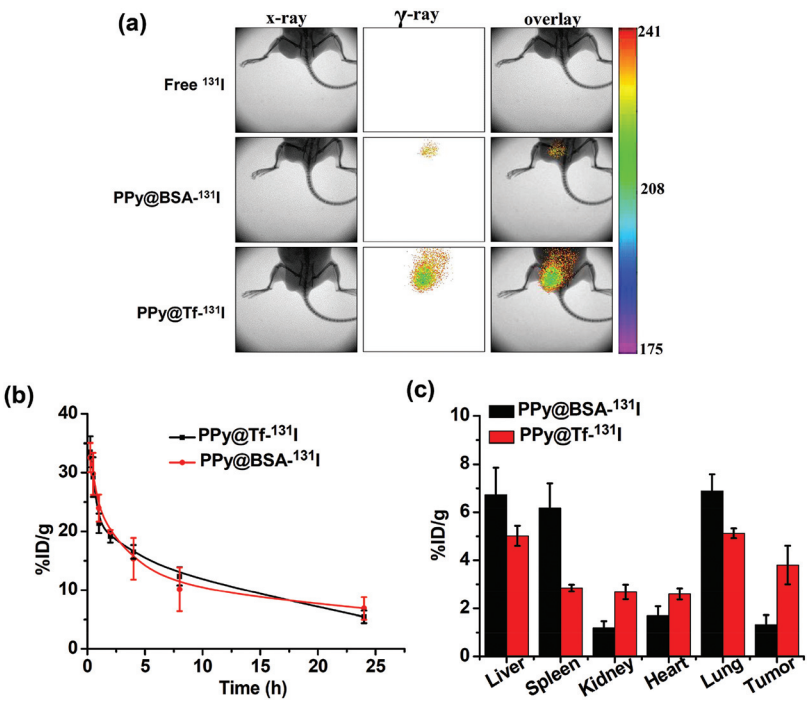

Fig. 3 *In vivo* behaviors of PPy@Tf-^{131}I. (a) Gamma imaging of U87MG tumor-bearing mice taken 24 h after the i.v. injection of free ^{131}I, PPy@BSA-^{131}I, or PPy@Tf-^{131}I. (b) Blood circulation curves of PPy@BSA-^{131}I and PPy@Tf-^{131}I after i.v. injection as determined by a gamma counter at different time points post-injection. (c) The biodistribution of Py@BSA-^{131}I and PPy@Tf-^{131}I after i.v injection for 24 h. The unit is the percentage of the injected dose per gram tissue (% ID g^{-1}).

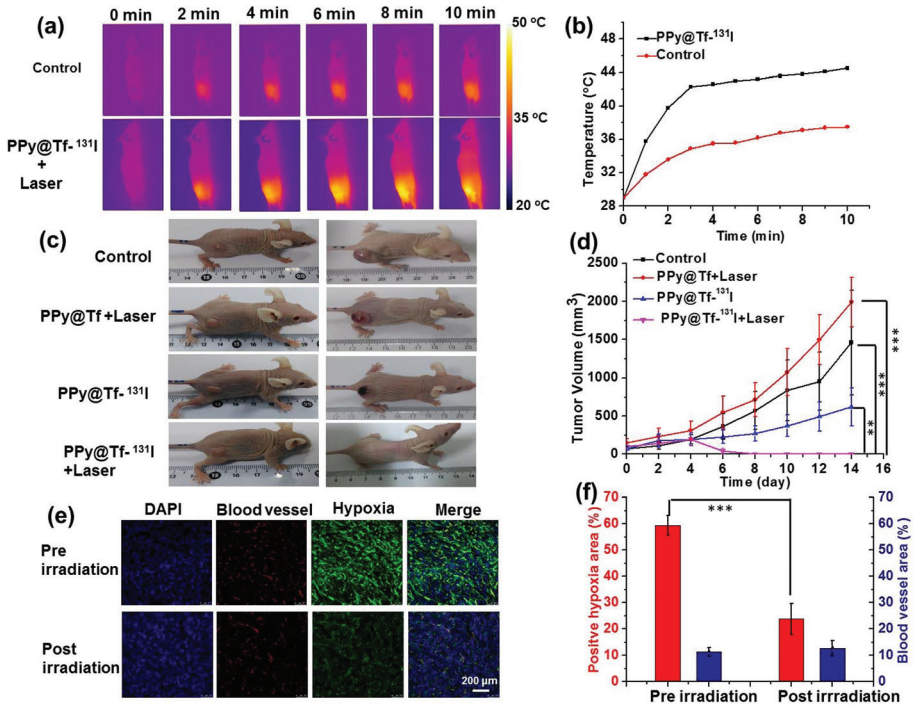

Fig. 4 *In vivo* combination therapy. (a) IR thermal images of U87MG tumor-bearing mice under the 808 nm laser irradiation (0.5 W cm^{-2}). (b) Tumor temperature changes monitored by the IR thermal camera during the laser irradiation of mice as indicated in (a). (c) Tumor growth curves of different groups of mice after various treatments indicated. (d) Representative photos of mice after various treatments taken at day 10. (e) Representative immunofluorescence images of tumor slices stained by the Hypoxyprobe™. The blood vessels and hypoxia areas were stained with anti-CD31 antibody (red), and anti-pimonidazole antibody (green), respectively. (f) Quantification of tumor hypoxia and blood vessel densities for different groups shown in (e). *P* values: $^{**}P < 0.01$, $^{***}P < 0.001$, ANOVA.

using a thermal camera (Fig. 4a & b). Then, the tumor sizes were measured using a digital caliper since the beginning of the treatment. Compared to the partially inhibited tumor growth in the mice treated with either PTT alone or RIT alone, the tumor growth on the mice treated by the combination therapy (PPy@Tf-^{131}I plus NIR laser) was most effectively inhibited, with only scars left on day 8 and no recurrence observed during the following days (Fig. 4c & d).

One critical factor that determines the efficacy of the radiation-induced damage of tumors is their oxygenation status, as oxygen molecules within tumor cells would react with radiation-induced DNA breaks to prevent DNA repairing by cells and enhance radiation-induced cell killing. The tumor hypoxia, a hallmark of solid tumors, would therefore lead to the resistance of tumors to radiation therapies. In our previous report, it has been found that the mild photothermal heating of tumors could efficiently relieve the tumor hypoxia by boosting the intra-tumoral blood flow,[15,16] making the tumor cells more vulnerable to the radiation therapy. As revealed by the *ex vivo* immunofluorescence staining of tumor slices in our experiments, tumors in mice injected with PPy@Tf after NIR-induced photothermal heating indeed showed obviously relieved tumor hypoxia (Fig. 4e). After laser irradiation, the percentage of the hypoxia positive area dropped from~60% for tumors in the untreated group to ~23% for tumors in mice after the mild photothermal treatment with PPy@Tf (Fig. 4f). Therefore, the excellent synergistic effect achieved in the combined PTT–RIT with PPy@Tf-^{131}I is likely owing to the improved tumor oxygenation after the mild PTT to overcome the hypoxia-associated resistance of tumors to RIT.

Finally, the potential *in vivo* toxicity of PPy@Tf-^{131}I was also investigated. No obvious sign of the toxic effect was observed in the PPy@Tf-^{131}I injected mice in our experiments after the PTT–RIT treatment within 14 days. The hematoxylin and eosin (H&E) stained images of all major organs of mice showed no noticeable organ damage or inflammatory lesion 14 days after such treatment with PPy@Tf-^{131}I (ESI, Fig. S6†), indicating that the PPy@Tf-^{131}I nanoparticles were not obviously toxic to the treated animals at our experimental dose.

Conclusions

In summary, we developed multifunctional PPy@Tf-^{131}I nanoparticles for tumor-targeted cancer combination therapy *via* a simple one-step synthesis method. Compared with PPy@BSA-^{131}I nanoparticles, the as-prepared PPy@Tf-^{131}I nanoparticles exhibited significantly increased cellular uptake and thus improved *in vitro* RIT efficacy. Such PPy@Tf-^{131}I nanoparticles were found to have a long blood circulation time and efficient tumor-targeted accumulation, which was 3-fold higher than the passive tumor accumulation of PPy@^{131}I-BSA

nanoparticles. Moreover, by utilizing the mild photothermal treatment induced tumor hypoxia relieving, the as-prepared PPy@Tf-^{131}I nanoparticles showed excellent synergistic therapeutic efficacy. Collectively, such PPy@Tf-^{131}I nanoparticles demonstrate several promising features as multifunctional nano-theranostics: (1) its one-step synthesis without needing further surface modification is very convenient and promising for reliable scale-up production; (2) PPy is known to show great biocompatibility while Tf is a natural protein without much safety concerns; (3) the Tf mediated active targeting ability could significantly improve the tumor specific accumulation of such PPy@Tf-^{131}I nanoparticles; (4) the excellent photothermal conversion ability of PPy could be exploited to remarkably relieve the tumor hypoxia, subsequently contributing to excellent synergistic cancer treatment outcomes in the combined photothermal-radioisotope therapy.

Materials and experiments

Materials

Bovine serum albumin (BSA) was purchased from J&C chemical Co. Transferrin and pyrrole monomer were purchased from Sigma-Aldrich. Ferric chloride hexahydrate ($FeCl_3 \cdot 6H_2O$) was purchased from Sinopharm Chemical Reagent Co., Ltd. Radionuclide ^{131}I was purchased from Shanghai GMS Pharmaceutical Co., Ltd. All cell-culture-related reagents were purchased from Hyclone.

Synthesis of ^{131}I-Trf@PPy and ^{131}I-BSA@PPy

To prepare ^{131}I-Tf, 10 mg of native Tf dissolved in 2 ml phosphate buffered saline (PBS) was mixed with 650 μCi of Na^{131}I and 0.1 mg of chloramine-T. After being stirred for 10 min at room temperature, excess ^{131}I was removed by ultra-filtration through an Amico filter device with a molecular weight cut-off (MWCO) of 10 kDa and washed with PBS three times. The final radiolabeling yield was calculated to be about 90%. Besides, ^{131}I-BSA was prepared by adopting the same procedure for the preparation of ^{131}I-Tf.

To prepare PPy@^{131}I-Tf or PPy@Tf nanoparticles, 10 mg ^{131}I-Tf or unlabeled Tf dissolved in 2 mL water was mixed with 5 μL of pyrrole monomer followed by 1 h stirring at room temperature. Then, 5 mg ferric chloride hexahydrate was added into the reaction mixture and reacted at room temperature for an additional 24 h. The final products were purified by ultra-filtration using an Amico filter device with a MWCO of 100 kDa. Free Tf was completely removed as checked by measuring the amount of Tf in the upper and lower solution by the bicinchoninic acid (BCA) assay. The nanoparticles were re-dissolved in PBS for future use. We measured the amount of Tf in the upper and lower solution by BCA assays. The results could confirm that free Tf was completely removed. PPy@^{131}I-BSA and PPy@BSA nanoparticles were prepared by the same procedure.

The morphology, size distribution and UV-vis-NIR spectrum of PPy@Tf nanoparticles were recorded using a TEM (Tecnai F20, FEI), a Malvern zetasizer (nano-ZS90) and a UV-vis-NIR spectrometer (Thermo Fisher), respectively. The photothermal conversion ability was monitored by using a thermal camera (Fotric 226).

Cellular experiments

Human glioblastoma U87MG cells were cultured in DMEM low-glucose medium containing 10% fetal bovine serum and 1% penicillin/streptomycin at 37 °C under 5% CO_2.

The *in vitro* active targeting ability of PPy@Tf-^{131}I nanoparticles was evaluated by using CLSM and flow cytometry. PPy@Tf-FITC and PPy@Tf-FITC nanoparticles were firstly prepared by using the same procedure for the preparation of PPy@Tf-^{131}I and PPy@BSA-^{131}I nanoparticles, with FITC labeled Tf and BSA used as the stabilizers during the synthesis of PPy, respectively. For CLSM observation, U87-MG cells were seeded in a 24 well plate containing circle glass coverslides at a density of 2×10^4 cells per well. 24 h later, one group of cells was incubated with PPy@BSA-FITC nanoparticles, while the other two groups of cells were incubated with PPy@Tf-FITC nanoparticles with one of them being pre-incubated with native Tf at a concentration of 0.5 mg mL^{-1} for 1 h. After being incubated for the designated periods of time, the cells were washed with PBS, fixed with 4% paraformaldehyde solution, stained with 4,6-diamino-2-phenyl indole (DAPI), and finally observed under the CLSM (Leica TCS-SP5II, Germany).

For flow cytometric analysis, 5×10^5 of U87MG cells were seeded in a 35 mm petri-dish and cultured at 37 °C for 24 h. Then, the cells which received the same treatments as aforementioned for CLSM observation were washed three times with PBS, trypsinized and re-dispersed in 1% BSA containing PBS for flow cytometric analysis (BD Calibur).

For targeted RIT, U87MG cells were seeded into 96-well cell culture plates until adherent and then incubated with various concentrations of free ^{131}I, PPy@Tf-^{131}I and PPy@BSA-^{131}I nanoparticles. After 1 h of incubation, free materials were removed by washing twice with fresh culture medium. Afterwards, the cells were re-incubated in fresh medium for additional 24 h before the MTT assay to determine the relative cell viabilities.

For PTT, U87MG cells were seeded into 96-well cell culture plates until adherent, incubated with different concentrations of PPy@Tf, and then exposed to the 808 nm laser (0.5 W cm^{-2}, 5 min). Afterwards, the MTT assay was carried out to determine the cell viabilities relative to the control untreated cells.

For combination therapy, U87MG cells were incubated with PPy@Tf-^{131}I and PPy@Tf at the same concentration of ^{131}I or PPy. For RIT, the cells were incubated with the PPy@Tf-^{131}I nanoparticles for 24 h. For PTT, the cells were incubated with PPy@Tf and placed under 808 nm laser irradiation at 0.5 W cm^{-2} for 5 min. Afterwards, the samples were incubated for 24 h. For combination therapy, the cells were incubated with PPy@Tf-^{131}I, exposed to the 808 nm laser (0.5 W cm^{-2}, 5 min) and then incubated for another 24 h. The MTT assay was carried out to determine the cell viabilities relative to the control untreated cells.

Tumor model

Female nude mice were purchased from Nanjing Peng Sheng Biological Technology Co, Ltd. All the animal experiments were performed in compliance with the Animal Management Rules of the Ministry of Health of the People's Republic of China (document no. 55, 2001) and under the guidelines for the Care and Use of Laboratory Animals of Soochow University Laboratory Animal Center. We also confirm that all experiments with live subjects were approved by Soochow University. The tumor model was created by subcutaneous injection of 1×10^6 U87MG cells in 50 μL of PBS. When the tumor volume reached ~75 mm^3, the mice were used for our following experiments.

Gamma imaging

Mice bearing U87MG tumors were i.v. injected with free ^{131}I, PPy@Tf-^{131}I and PPy@BSA-^{131}I nanoparticles (300 μCi of ^{131}I) and imaged at 24 h post-injection by using an *in vivo* animal imaging system (Kodak).

Blood circulation and biodistribution

Nude mice bearing U87MG tumors were i.v. injected with PPy@Tf-^{131}I and PPy@BSA-^{131}I nanoparticles, respectively (300 μCi of ^{131}I). Blood samples (~20 μl) were withdrawn from mice at different time points, and their radioactivities were measured by using a gamma counter (Science and Technology Institute of China in Jia Branch Innovation Co., Ltd). Their major organs including the liver, spleen, kidney, heart, lung and tumor were collected at 24 h post-injection (p.i.), weighed and measured by using the gamma counter.

Combination therapy

Mice bearing U87MG tumors were randomly divided into four groups (n = 6 per group) for various treatments. Two groups of mice were i.v. injected with saline and PPy@Tf nanoparticles, respectively, while the other two groups of mice received i.v. injection of PPy@Tf-^{131}I nanoparticles (300 μCi per mouse). At 24 h post-injection, the tumors in the group of mice with the PPy@Tf nanoparticle injection and one group of mice with PPy@Tf-^{131}I nanoparticles were exposed to the 808 nm laser (0.5 W cm^{-2}, 20 min), with their tumor surface temperature maintained at about 45–46 °C as monitored by using an infrared camera (Fotric 226). The tumor sizes were monitored every 2 days using a digital caliper and the tumor volume was calculated according to the following equation: volume = $width^2 \times length/2$.

Acknowledgements

This work was partially supported by the National Research Programs from the Ministry of Science and Technology (MOST) of China (2016YFA0201200), the National Natural Science Foundation of China (51525203), the Collaborative Innovation Center of Suzhou Nano Science and Technology, Postgraduate research and innovation projects in Jiangsu Province (KYZZ15 0321), and a Project Funded by the Priority Academic Program Development (PAPD) of Jiangsu Higher Education Institutions.

References

1 X. D. Zhang, Z. Luo, J. Chen, X. Shen, S. Song, Y. Sun, S. Fan, F. Fan, D. T. Leong and J. Xie, *Adv. Mater.*, 2014, **26**(26), 4565–4568.
2 X.-Y. Su, P.-D. Liu, H. Wu and N. Gu, *Cancer Biol. Med.*, 2014, **11**(2), 86–91.
3 G. Liu, S. Dou, G. Mardirossian, J. He, S. Zhang, X. Liu, M. Rusckowski and D. J. Hnatowich, *Clin. Cancer Res.*, 2006, **12**(16), 4958–4964.
4 J. C. Blasko, P. D. Grimm, J. E. Sylsvester and W. Cavanagh, *Radiother. Oncol.*, 2000, **57**(3), 273–278.
5 Y. Chao, G. Wang, C. Liang, X. Yi, X. Zhong, J. Liu, M. Gao, K. Yang, L. Cheng and Z. Liu, *Small*, 2016, **12**(29), 3967–3975.
6 X. Zhong, K. Yang, Z. Dong, X. Yi, Y. Wang, C. Ge, Y. Zhao and Z. Liu, *Adv. Funct. Mater.*, 2015, **25**(47), 7327–7336.
7 H. Hong, Y. Zhang, J. Sun and W. Cai, *Nano Today*, 2009, **4**(5), 399–413.
8 M. S. Muthu and B. Wilson, *Nanomedicine*, 2010, **5**(2), 169–171.
9 L. Zhang, H. Chen, L. Wang, T. Liu, J. Yeh, G. Lu, L. Yang and H. Mao, *Nanotechnol., Sci. Appl.*, 2010, **3**, 159–170.
10 M. Zhou, Y. Chen, M. Adachi, X. Wen, B. Erwin, O. Mawlawi, S. Y. Lai and C. Li, *Biomaterials*, 2015, **57**, 41–49.
11 J. Shi, D. Fan, C. Dong, H. Liu, B. Jia, H. Zhao, X. Jin, Z. Liu, F. Li and F. Wang, *Theranostics*, 2014, **4**(3), 256.
12 S. A. Gulec, K. Pennington, J. Wheeler, T. C. Barot, R. R. Suthar, M. Hall and D. Schwartzentruber, *Am. J. Clin. Oncol.*, 2013, **36**(5), 455–460.
13 A. Dietrich, L. Koi, K. Zöphel, W. Sihver, J. Kotzerke, M. Baumann and M. Krause, *Br. J. Radiol.*, 2015, **88**(1051), 20150042.
14 C.-L. Peng, Y.-H. Shih, P.-C. Lee, T. M.-H. Hsieh, T.-Y. Luo and M.-J. Shieh, *ACS Nano*, 2011, **5**(7), 5594–5607.
15 G. Song, C. Liang, H. Gong, M. Li, X. Zheng, L. Cheng, K. Yang, X. Jiang and Z. Liu, *Adv. Mater.*, 2015, **27**(40), 6110–6117.
16 X. Yi, K. Yang, C. Liang, X. Zhong, P. Ning, G. Song, D. Wang, C. Ge, C. Chen and Z. Chai, *Adv. Funct. Mater.*, 2015, **25**(29), 4689–4699.
17 L. Chen, X. Zhong, X. Yi, M. Huang, P. Ning, T. Liu, C. Ge, Z. Chai, Z. Liu and K. Yang, *Biomaterials*, 2015, **66**, 21–28.
18 W. Cai and H. Hong, *Am. J. Nucl. Med. Mol. Imaging*, 2012, **2**(2), 136–140.
19 J. Zhou, M. Yu, Y. Sun, X. Zhang, X. Zhu, Z. Wu, D. Wu and F. Li, *Biomaterials*, 2011, **32**(4), 1148–1156.
20 L. Brannon-Peppas and J. O. Blanchette, *Adv. Drug Delivery Rev.*, 2012, **64**, 206–212.

21 J. D. Byrne, T. Betancourt and L. Brannon-Peppas, *Adv. Drug Delivery Rev.*, 2008, **60**(15), 1615–1626.
22 Q. Zhang, X. Wang, P. Z. Li, K. T. Nguyen, X. J. Wang, Z. Luo, H. Zhang, N. S. Tan and Y. Zhao, *Adv. Funct. Mater.*, 2014, **24**(17), 2450–2461.
23 K. S. Oh, H. Lee, J. Y. Kim, E. J. Koo, E. H. Lee, J. H. Park, S. Y. Kim, K. Kim, I. C. Kwon and S. H. Yuk, *J. Controlled Release*, 2013, **165**(1), 9–15.
24 W. Wu, S. Wieckowski, G. Pastorin, M. Benincasa, C. Klumpp, J. P. Briand, R. Gennaro, M. Prato and A. Bianco, *Angew. Chem., Int. Ed.*, 2005, **44**(39), 6358–6362.
25 J. Geng, C. Sun, J. Liu, L. D. Liao, Y. Yuan, N. Thakor, J. Wang and B. Liu, *Small*, 2015, **11**(13), 1603–1610.
26 L. Dou, Y. Liu, Z. Hong, G. Li and Y. Yang, *Chem. Rev.*, 2015, **115**(23), 12633–12665.
27 Y. Yuan, J. Liu and B. Liu, *Angew. Chem., Int. Ed.*, 2014, **53**(28), 7163–7168.
28 X. Liang, Y. Li, X. Li, L. Jing, Z. Deng, X. Yue, C. Li and Z. Dai, *Adv. Funct. Mater.*, 2015, **25**(9), 1451–1462.
29 X. Song, Q. Chen and Z. Liu, *Nano Res.*, 2015, **8**(2), 340–354.
30 B.-P. Jiang, L. Zhang, Y. Zhu, X.-C. Shen, S.-C. Ji, X.-Y. Tan, L. Cheng and H. Liang, *J. Mater. Chem. B*, 2015, **3**(18), 3767–3776.
31 X. Song, C. Liang, H. Gong, Q. Chen, C. Wang and Z. Liu, *Small*, 2015, **11**(32), 3932–3941.
32 K. Wang, Y. Zhang, J. Wang, A. Yuan, M. Sun, J. Wu and Y. Hu, *Sci. Rep.*, 2016, **6**, 27421.
33 Y. Li, H. He, X. Jia, W.-L. Lu, J. Lou and Y. Wei, *Biomaterials*, 2012, **33**(15), 3899–3908.
34 Q. Xu, Y. Liu, S. Su, W. Li, C. Chen and Y. Wu, *Biomaterials*, 2012, **33**(5), 1627–1639.
35 A. Salvati, A. S. Pitek, M. P. Monopoli, K. Prapainop, F. B. Bombelli, D. R. Hristov, P. M. Kelly, C. Åberg, E. Mahon and K. A. Dawson, *Nat. Nanotechnol.*, 2013, **8**(2), 137–143.
36 M. S. Muthu, R. V. Kutty, Z. Luo, J. Xie and S.-S. Feng, *Biomaterials*, 2015, **39**, 234–248.
37 D. Roy, G. Y. Berguig, B. Ghosn, D. D. Lane, S. Braswell, P. S. Stayton and A. J. Convertine, *Polym. Chem.*, 2014, **5**(5), 1791–1799.
38 C. H. J. Choi, C. A. Alabi, P. Webster and M. E. Davis, *Proc. Natl. Acad. Sci. U. S. A.*, 2010, **107**(3), 1235–1240.